

DECLARATION

I declare that the thesis entitled, A SIMULATION STUDY OF COLLECTIVE BEHAVIOUR OF HADRONIC MATTER AT FAIR ENERGIES, has been prepared by me under the guidance of Prof. Amitabha Mukhopadhyay, Department of Physics, University of North Bengal. No part of this thesis has been formed on the basis of any previously awarded degree or fellowship.

Date: 27/12/2021

Soumya Sarkar

Soumya Sarkar

Department of Physics
University of North Bengal
Siliguri 734 013, Darjeeling, India

CERTIFICATE

This is to certify that the work contained in the thesis titled " A SIMULATION STUDY OF COLLECTIVE BEHAVIOUR OF HADRONIC MATTER AT FAIR ENERGIES" submitted by Mr. Soumya Sarkar, has been carried out in the Department of Physics, University of North Bengal under my supervision. This work has not been submitted elsewhere for any degree/diploma.

Date: 27/12/2021

Amitabha Mukhopadhyay








Prof. Amitabha Mukhopadhyay
Supervisor

Department of Physics
University of North Bengal
Siliguri 734013, West Bengal, India

Document Information

Analyzed document	Soumya Sarkar_Physics.pdf (D123562954)
Submitted	2021-12-23T08:58:00.0000000
Submitted by	University of North Bengal
Submitter email	nbuplg@nbu.ac.in
Similarity	1%
Analysis address	nbuplg.nbu@analysis.arkund.com

Sources included in the report

W	URL: https://drupal.star.bnl.gov/STAR/files/thesis_Rihan_Haque.pdf Fetched: 2021-11-03T15:04:36.5730000	 9
J	URL: e55b8639-610b-40af-970e-44e4d725c2ae Fetched: 2019-02-19T01:28:30.1470000	 2
W	URL: https://arxiv.org/pdf/2111.05248 Fetched: 2021-11-23T20:02:59.8530000	 1
W	URL: https://www.math.ucdavis.edu/~linear/linear-guest.pdf Fetched: 2020-03-21T17:02:05.8870000	 1
W	URL: https://www.science.gov/topicpages/u/ultrarelativistic+heavy-ion+collisions Fetched: 2021-11-08T08:20:36.0970000	 1
W	URL: https://d-nb.info/1043978305/34 Fetched: 2021-07-14T12:31:20.0970000	 1
W	URL: https://en.wikipedia.org/wiki/Pseudorapidity Fetched: 2020-01-17T23:52:25.3400000	 1

Acknowledgments

I would like to take this opportunity to express my sincere appreciation for all those who have supported, encouraged, and inspired me in the pursuit of my research work. My thesis work would have not been possible without the support and encouragement from my teachers, colleagues, friends and family members. First and foremost, I would like to thank my supervisor Prof. Amitabha Mukhopadhyay of the Physics Department of North Bengal University for teaching me many Physics courses in the post-graduate level, and also for guiding my Ph.D. research. My interactions with him during the past several years has been a great experience. His constructive criticism on my research work was essential for a successful completion of this thesis. I would like to express my sincere gratitude to Dr. Provash Mali of the Physics Department of North Bengal University for his constant help and support, particularly at the beginning of my research career in the area of computational work and in developing software. I also acknowledge the discussions that on several occasions I had with Prof. Subhasis Chattopadhyay and Dr. Partha Pratim Bhaduri, both from the Variable Energy Cyclotron Centre, Kolkata, during my stay there at the early stages of my research career. My heartfelt gratitude goes to Mr. Sanjib Kumar Manna, Mr. Somnath Ghosh and especially to Mr. Joydeep Thakur, research students of the Physics Department of North Bengal University, for maintaining an enjoyable working atmosphere in the laboratory and for their very warm hearted help and support. It is also a great pleasure to thank all my colleagues at the Siliguri College. Finally and most importantly, I would like to convey my deepest sense of gratitude to my family for the much and often needed moral support, which has kept me going.

Soumya Sarkar

*Dedicated to the memory of
My Father*

List of Tables

1.1	Chronological commissioning of HIC accelerator facilities (past and present).	7
1.2	Physics issues and their corresponding observables for the CBM experiment.	36
2.1	N_{part} , N_{coll} at different centrality (in %) as obtained from MCG model in Au+Au collisions at $E_{\text{lab}} = (10 - 40)A$ GeV and central particle density estimated from AMPT(default), AMPT(string melting) and UrQMD model.	53
2.2	Centroid of the pseudorapidity distribution (η_0) in Au+Au collisions corresponding to different energies (in GeV) as obtained from the AMPT (default), AMPT(string melting) and UrQMD model.	55
2.3	Fit parameters of Equation (2.12) as obtained at different energies for AMPT (default), AMPT (string melting), and UrQMD model.	59
2.4	The values of kinetic freeze-out temperature T_{kin} (in MeV) and square of radial flow velocity $\langle\beta_T\rangle^2$ (in c^2) for the 0 – 5% most central Au+Au events corresponding to different energies for the AMPT (default), AMPT (string melting), and UrQMD models.	62
3.1	N_{coll} , N_{part} , S , $\varepsilon_2^{\text{std}}$, $\varepsilon_2^{\text{part}}$ and ε_3 at different centralities in Au+Au collision at $E_{\text{lab}} = 30A$ GeV obtained from the MCG simulation.	75
5.1	N_{part} dependence of the asymmetry parameters and midrapidity particle densities in different colliding systems at $E_{\text{lab}} = 30A$ GeV.	124
7.1	Limiting values of transverse sphericity for jetty and isotropic events	152

List of Figures

1.1	Measurements of the strong field coupling constant (α_s) against energy-momentum transfer Q . Lines refer to the perturbative QCD prediction which are in excellent agreement with the experiments. The figure is taken from [8].	2
1.2	A probable timeline of the universe since Big Bang [21].	5
1.3	A typical nucleus-nucleus interaction before and after the collision. Particles are produced in the participants' zone, while the spectators remain uninfluenced. The figure is taken from Ref. [23].	8
1.4	Schematic exemplar of different stages of a heavy-ion collision, the <i>Little Bang</i> . The figure is taken from Ref. [26]	10
1.5	Space time evolution of a high-energy collision between two nuclei in their CM frame, (a) without and (b) with QGP formation. The figure is taken from Ref. [27].	11
1.6	A schematic of the QCD phase diagram showing locations of different states of hadronic/partonic matter [51].	19
1.7	Centrality dependence of J/ψ R_{AA} . This figure is taken from Ref. [56].	22
1.8	Left: Schematic of di-jet production. Right: Distribution of azimuthal angle difference between trigger and associated particles at STAR from central Au+Au, d+Au, and p+p collisions. The figure is taken from Ref. [62].	23
1.9	R_{AA} values for jets considering two different p_T intervals at midrapidity as a function of N_{part} . The figure is taken from Ref. [63].	23
1.10	Strangeness enhancements at midrapidity as a function of N_{part} , showing LHC, RHIC and SPS data simultaneously. The figure is taken from Ref. [66].	24
1.11	Schematic of initial space anisotropy w.r.t the reaction ($x - z$) plane being converted into momentum space anisotropy due to in-medium interactions among the final state hadrons.	27
1.12	First measurement of in-plane elliptic flow by the E877 Collaboration at 11.8A Gev [74]. The solid line is a distribution with Fourier coefficients v_0, v_1, v_2 at three different pseudorapidity.	28

1.13	Elliptic flow at midrapidity in 20 – 30% centrality bin as a function of energy from FOPI, AGS, SPS, RHIC to LHC. The basic figure is taken from [76] except certain textual changes.	29
1.14	Elliptic flow as a function of centrality defined as n_{ch}/n_{max} reported by STAR Collaboration at $\sqrt{s_{NN}} = 130$ GeV [77]. The open rectangles show a range of values expected for v_2 in the hydrodynamic limit, scaled from ε , the initial space eccentricity of the overlap region.	29
1.15	Elliptic flow integrated over the p_T range $0.2 < p_T < 5.0$ GeV/c at $\sqrt{s_{NN}} = 2.76$ TeV as a function of centrality [78]. RHIC measurements at $\sqrt{s_{NN}} = 200$ GeV is integrated over the p_T range $0.15 < p_T < 5.0$ GeV/c.	30
1.16	p_T dependence of $v_2\{4\}$ at $\sqrt{s_{NN}} = 2.76$ TeV for various centralities compared to STAR measurements at $\sqrt{s_{NN}} = 200$ GeV [78].	30
1.17	Left: Differential elliptic flow at RHIC ($\sqrt{s_{NN}} = 200$ GeV) as a function of transverse momentum compared to hydrodynamical predictions [81]. Right: Hydrodynamical prediction of differential elliptic flow for 20 – 30% centrality at $\sqrt{s_{NN}} = 200$ GeV (dashed lines) and $\sqrt{s_{NN}} = 2.76$ TeV (solid lines) [80].	31
1.18	Left: v_2 against transverse kinetic energy (KE_T) for different species for minimum bias Au+Au collisions at $\sqrt{s_{NN}} = 200$ GeV. Right: Same but after scaling by NCQ. The figure is taken from [84].	32
1.19	Eccentricity scaled v_2 as a function of particle density in the transverse plane at AGS, SPS to RHIC. The figure is from Ref. [88].	33
1.20	Difference in v_2 for particles and their corresponding anti-particles measured by the STAR collaboration at RHIC for 0 – 80% central events. Dashed lines are fits to some power law function, the details of which can be found in [89].	33
1.21	Transverse momentum dependence of different order flow harmonics (v_n) estimated by the ALICE Collaboration. [93].	34
1.22	Left: Hadronic freeze out line on the temperature versus net-baryon density plane as obtained in statistical model [98]. Right: Interaction rate reached by existing and future heavy-ion experiments as a function of beam energy [99].	35
2.1	Charged hadron multiplicity distribution in Au+Au collisions at $E_{lab} = (10 - 40)A$ GeV.	52
2.2	Impact parameter dependence of N_{part} and N_{coll} in Au+Au collisions at $E_{lab} = (10 - 40)A$ GeV.	54
2.3	Azimuthal angle distribution of charged hadrons at midrapidity in Au+Au collisions at $E_{lab} = (10 - 40)A$ GeV.	54
2.4	Pseudorapidity distribution of charged hadrons in Au+Au collisions at $E_{lab} = (10 - 40)A$ GeV.	55

2.5	Variation of $dN_{\text{ch}}/d\eta$ with η for 0 – 5% central Au+Au collisions at $E_{\text{lab}} = (10 - 40)A$ GeV.	56
2.6	Variation of $\langle p_T \rangle$ of charged hadrons with η in Au+Au collisions at $E_{\text{lab}} = (10 - 40)A$ GeV.	56
2.7	Centrality dependence of the integrated yield of charged hadrons per participant pair at midrapidity in Au+Au collisions at $E_{\text{lab}} = (10 - 40)A$ GeV. The solid lines represent the fit following Equation (2.12).	58
2.8	Transverse momentum spectra of all charged hadrons at midrapidity in Au+Au collisions at $E_{\text{lab}} = (10 - 40)A$ GeV. For clarity the UrQMD and AMPT (default) results are scaled with appropriate factors.	60
2.9	Transverse mass spectra for pion, kaon and proton at midrapidity for 0 – 5% central Au+Au collisions at $E_{\text{lab}} = 30A$ GeV. The UrQMD and AMPT (default) results are scaled properly for clarity.	60
2.10	Hadronic mass dependence of effective temperature for 0 – 5% central Au+Au collisions at $E_{\text{lab}} = (10 - 40)A$ GeV. The solid lines are linear fit following Equation (2.14). The NA49 points are taken from [40]	61
2.11	Average transverse momentum of charged hadrons at midrapidity plotted against centrality in Au+Au collisions at $E_{\text{lab}} = (10 - 40)A$ GeV.	62
3.1	Left: Schematic of a non-central heavy-ion collision in the transverse plane [16]. Right: v_2 scaled by ε_{std} as a function of N_{part} [4].	68
3.2	Left: Schematic of a heavy-ion collision illustrating the reaction plane and participant plane. Right: v_2 scaled by $\varepsilon_{\text{part}}$ as a function of N_{part} [4].	69
3.3	Exemplar of elliptic and triangular anisotropies generated after a collision between two nuclei. The pink circles represent the participating nucleons. The figure is taken from [18]	70
3.4	Centrality dependence of ε_n of the overlapping region for Au+Au collision at $E_{\text{lab}} = 30A$ GeV.	74
3.5	Centrality dependence of the elliptic flow parameter of charged hadrons at midrapidity in Au+Au collision at $E_{\text{lab}} = (10 - 40)A$ GeV without considering initial fluctuations. Experimental data points are from [9].	77
3.6	$v_2/\varepsilon_2^{\text{std}}$ as a function of N_{part} for the charged hadrons at midrapidity in Au+Au collisions at $E_{\text{lab}} = (10 - 40)A$ GeV without considering initial fluctuations.	78
3.7	Centrality dependence of elliptic flow of charged hadrons at midrapidity in Au+Au collision at $E_{\text{lab}} = (10 - 40)A$ GeV after considering initial fluctuations. Experimental data points are from Ref. [9].	79

3.8	$v_2/\varepsilon_2^{\text{part}}$ as a function of N_{part} for the charged hadrons at midrapidity in Au+Au collisions at $E_{\text{lab}} = (10-40)A$ GeV after considering initial fluctuations.	80
3.9	Variation of scaled elliptic flow with scaled particle density.	81
3.10	Centrality dependence of triangular flow of charged hadrons at midrapidity in Au+Au collision at $E_{\text{lab}} = (10-40)A$ GeV	83
3.11	v_3/ε_3 as a function of N_{part} for the charged hadrons at midrapidity in Au+Au collisions at $E_{\text{lab}} = (10-40)A$ GeV.	83
3.12	v_3/v_2 -ratio computed at midrapidity plotted as a function of N_{part} in different p_T intervals in Au+Au collision at $E_{\text{lab}} = 30A$ GeV for the AMPT (string melting) model simulation (upper panel). The v_3/v_2 -ration for a p_T interval is scaled by the corresponding ratio for the entire p_T -range ($0 \leq p_T \leq 2.0$ GeV/c) (lower panel).	85
3.13	v_2 and v_2/ε_2 plotted against p_T for charged hadrons at midrapidity in Au+Au collisions at $E_{\text{lab}} = 10A$ GeV. v_2 for the last two centralities are slightly shifted for clarity.	86
3.14	Same as in Figure 3.13 but at $E_{\text{lab}} = 20A$ GeV.	86
3.15	Same as in Figure 3.13 but at $E_{\text{lab}} = 30A$ GeV. The available experimental results (STAR data) are shown by continuous curves.	87
3.16	Same as in Figure 3.13 but at $E_{\text{lab}} = 40A$ GeV.	87
3.17	v_3 and v_3/ε_3 plotted against p_T for charged hadrons at midrapidity in Au+Au collisions at $E_{\text{lab}} = 10A$ GeV.	89
3.18	Same as in Figure 3.17 but at $E_{\text{lab}} = 20A$ GeV.	89
3.19	Same as in Figure 3.17 but at $E_{\text{lab}} = 30A$ GeV.	90
3.20	Same as in Figure 3.17 but at $E_{\text{lab}} = 40A$ GeV.	90
3.21	Species dependence of v_2 as a function of p_T at midrapidity for Au+Au collision at $E_{\text{lab}} = 30A$ GeV.	91
3.22	Species dependence of v_3 as a function of p_T at midrapidity for Au+Au collision at $E_{\text{lab}} = 30A$ GeV.	92
3.23	v_2 scaled by the constituent quark numbers of hadrons as a function of K_T/n_q at midrapidity for Au+Au collision at $E_{\text{lab}} = 30A$ GeV. The solid line is fitted following Equation (3.31).	93
3.24	v_3 scaled by the constituent quark numbers of hadrons as a function of K_T/n_q at midrapidity for Au+Au collision at $E_{\text{lab}} = 30A$ GeV. The solid line is fitted following Equation (3.31).	93
3.25	Comparison between particle-wise and event-wise averaged values of v_2 plotted against η in Au+Au collisions at $E_{\text{lab}} = (10-40)A$ GeV.	95

3.26	Comparison between particle-wise and event-wise averaged values of v_3 plotted against η in Au+Au collisions at $E_{\text{lab}} = (10 - 40)A$ GeV.	95
3.27	v_2 estimated by various techniques as a function of N_{part} at midrapidity in Au+Au collision at $E_{\text{lab}} = 30A$ GeV. $v_2\{\text{est}\}$ values are slightly shifted for clarity.	97
3.28	ε_2 estimated by various techniques as a function of N_{part} in Au+Au collision at $E_{\text{lab}} = 30A$ GeV. $\varepsilon_2\{\text{est}\}$ values are slightly shifted for clarity.	97
3.29	Centrality dependence of elliptic flow fluctuation and eccentricity fluctuation in Au+Au collisions at $E_{\text{lab}} = 30A$ GeV.	98
3.30	v_2 computed by various techniques and fluctuation in v_2 plotted against p_T for charged hadrons at midrapidity in Au+Au collisions at $E_{\text{lab}} = 30A$ GeV.	98
3.31	Relative v_2 fluctuation as a function of p_T . Experimental data points at RHIC are taken from [64, 65] and those at LHC from [66].	99
4.1	Centrality dependence of integrated yield of charged hadrons in Au+Au collisions at $E_{\text{lab}} = 30A$ GeV for different parton interaction cross sections.	105
4.2	Average transverse momentum of charged hadrons at midrapidity plotted against centrality in Au+Au collisions at $E_{\text{lab}} = 30A$ GeV for different parton interaction cross sections.	106
4.3	v_2 as a function of ε_2 in different N_{part} intervals for Au+Au collision at $E_{\text{lab}} = 30A$ GeV for different parton interaction cross sections.	107
4.4	v_3 as a function of ε_3 in different N_{part} intervals for Au+Au collision at $E_{\text{lab}} = 30A$ GeV for different parton interaction cross sections.	107
4.5	Centrality dependence of elliptic flow of charged hadrons at midrapidity in Au+Au collision at $E_{\text{lab}} = 30A$ GeV for different parton interaction cross sections. STAR data is taken from [3]	108
4.6	Centrality dependence of triangular flow of charged hadrons at midrapidity in Au+Au collision at $E_{\text{lab}} = 30A$ GeV for different parton interaction cross sections.	109
4.7	Elliptical flow scaled by eccentricity against centrality for different parton interaction cross sections at midrapidity for Au+Au collision at $E_{\text{lab}} = 30A$ GeV.	110
4.8	Triangular flow scaled by triangularity against centrality for different parton interaction cross sections at midrapidity in Au+Au collision at $E_{\text{lab}} = 30A$ GeV.	110
4.9	Elliptical flow scaled by eccentricity plotted against particle density in the transverse plane for Au+Au collision at $E_{\text{lab}} = 30A$ GeV for different parton interaction cross sections. Solid lines represent best fits to the data.	111

4.10	Triangular flow scaled by triangularity against $\sqrt{N_{\text{part}}}$ for different parton interaction cross sections at midrapidity in Au+Au collision at $E_{\text{lab}} = 30A$ GeV. Solid lines represent best fits to the data.	112
4.11	Dependence of v_3/v_2 on N_{part} in different p_T bins for Au+Au collision at $E_{\text{lab}} = 30A$ GeV for different parton interaction cross sections.	113
4.12	p_T dependence of v_2 for different centrality windows at midrapidity in Au+Au collision at $E_{\text{lab}} = 30A$ GeV for different parton interaction cross sections. STAR data is derived from [3].	114
4.13	p_T dependence of v_3 for different centrality windows at midrapidity in Au+Au collision at $E_{\text{lab}} = 30A$ GeV for different parton interaction cross sections.	115
4.14	NA49 data on p_T dependence of v_2 obtained from Pb+Pb interactions at 40A GeV compared with UrQMD and AMPT simulation (both default and string melting) for pions and protons at different partonic cross sections and at different centralities. The experimental values are shown as points, while corresponding simulations are shown by continuous curves.	116
4.15	Elliptic flow as a function of pseudorapidity for different parton interaction cross sections in Au+Au collision at $E_{\text{lab}} = 30A$ GeV.	117
4.16	Triangular flow as a function of pseudorapidity for different parton interaction cross sections in Au+Au collision at $E_{\text{lab}} = 30A$ GeV.	117
5.1	Multiplicity distribution of charged hadrons for different colliding systems at $E_{\text{lab}} = 30A$ GeV.	121
5.2	Eccentricity as a function of centrality measured in terms of N_{part}	122
5.3	Triangularity as a function of N_{part}	122
5.4	Distributions of v_1 of charged hadrons in the final state.	125
5.5	(Color online) Distributions of $v_2/\langle v_2 \rangle$ and $\varepsilon_2/\langle \varepsilon_2 \rangle$ of final state charged hadrons.	126
5.6	Distributions of $v_3/\langle v_3 \rangle$ and $\varepsilon_3/\langle \varepsilon_3 \rangle$ of final state charged hadrons.	126
5.7	N_{part} dependence of v_1 of charged hadrons for different colliding systems.	128
5.8	η dependence of v_1 of charged hadrons for different colliding systems.	128
5.9	p_T dependence of v_1 of charged hadrons for different colliding systems.	129
5.10	N_{part} dependence of (a) the elliptic flow parameter v_2 , (b) v_2 scaled by the standard eccentricity ε_{std} , and (c) v_2 scaled by the participant eccentricity $\varepsilon_{\text{part}}$, for charged hadrons in various AB collisions at $E_{\text{lab}} = 30A$ GeV.	131
5.11	Variation of eccentricity scaled elliptic flow with transverse particle density.	132
5.12	(a) Triangular flow and (b) triangular flow scaled by triangularity of charged hadrons against N_{part} for various AB collisions at $E_{\text{lab}} = 30A$ GeV.	133

5.13	Ratio of v_3 to v_2 of charged hadrons as a function of N_{part} for different colliding systems at $E_{\text{lab}} = 30A$ GeV.	134
5.14	p_T dependence of v_2 (upper panel) and v_2/ε_2 (lower panel) of charged hadrons for different colliding systems at $E_{\text{lab}} = 30A$ GeV.	135
5.15	p_T dependence of v_3 (upper panel) and v_3/ε_3 (lower panel) of charged hadrons for different colliding systems at $E_{\text{lab}} = 30A$ GeV.	135
6.1	Azimuthal distribution of (a) total radial velocity, (b) multiplicity, (c) mean radial velocity and (d) all the aforesaid quantities properly normalized for charged hadrons produced in Au+Au collisions at $E_{\text{lab}} = 40A$ GeV.	141
6.2	Centrality dependence of anisotropy parameter v_2 obtained from the azimuthal distributions of total radial velocity, multiplicity, and mean radial velocity in Au+Au collision at $E_{\text{lab}} = 10A$ and $40A$ GeV.	143
6.3	Centrality dependence of isotropic flow coefficient v_0 obtained from the azimuthal distributions of total radial velocity, multiplicity and mean radial velocity in Au+Au collision at $E_{\text{lab}} = 10A$ and $40A$ GeV.	144
6.4	Transverse momentum dependence of anisotropy parameter v_2 obtained from the azimuthal distributions of total radial velocity, multiplicity and mean radial velocity in Au+Au collision at $E_{\text{lab}} = 10A$ and $40A$ GeV.	145
6.5	Transverse momentum dependence of isotropic coefficient v_0 obtained from the azimuthal distributions of total radial velocity, multiplicity and mean radial velocity in Au+Au collision at $E_{\text{lab}} = 10A$ and $40A$ GeV.	146
7.1	Sphericity distribution of charged hadrons in Au+Au collision at $E_{\text{lab}} = 30A$ GeV.	151
7.2	p_T -spectra of different charged hadrons in the midrapidity region for isotropic, jetty and S_T -integrated events in 20–30% central Au+Au collisions at $E_{\text{lab}} = 30A$ GeV. Inset: Ratio of p_T -spectra for the isotropic and jetty events to S_T -integrated events.	153
7.3	Crossing point of the ratio of the p_T spectra of isotropic and jetty events to S_T -intergrated events as a function of particle mass in Au+Au collisions at $E_{\text{lab}} = 30A$ GeV.	153
7.4	N_{part} dependence of average p_T of different charged hadrons at midrapidity in isotropic, jetty and S_T integrated events in Au+Au collisions at $E_{\text{lab}} = 30A$ GeV.	154
7.5	Integrated yields in the midrapidity region of different charged hadrons as a function of N_{part} for the isotropic, jetty and S_T -integrated events in Au+Au collisions at $E_{\text{lab}} = 30A$ GeV.	155

7.6	Integrated yields in the midrapidity region of different charged hadrons per participant nucleon pair as a function of N_{part} for the isotropic, jetty and S_T -integrated events in Au+Au collision at $E_{\text{lab}} = 30A$ GeV.	156
7.7	Elliptic flow coefficient (v_2) as a function of N_{part} at midrapidity for isotropic, jetty and S_T -integrated events in Au+Au collisions at $E_{\text{lab}} = 30A$ GeV.	157
7.8	Triangular flow coefficient (v_3) as a function of N_{part} at midrapidity for isotropic, jetty and S_T integrated events in Au+Au collisions at $E_{\text{lab}} = 30A$ GeV.	158
7.9	Eccentricity (upper panel) and triangularity (lower panel) against N_{part} for isotropic, jetty and S_T -integrated events in Au+Au collisions at $E_{\text{lab}} = 30A$ GeV.	159
7.10	Elliptic flow coefficient (v_2) scaled by the eccentricity parameter (ε_2) plotted against N_{part} at midrapidity for isotropic, jetty and S_T -integrated events in Au+Au collisions at $E_{\text{lab}} = 30A$ GeV.	160
7.11	Triangular flow coefficient (v_3) scaled by the triangularity parameter (ε_3) plotted against N_{part} at midrapidity for isotropic, jetty and S_T -integrated events in Au+Au collisions at $E_{\text{lab}} = 30A$ GeV.	160
7.12	p_T -dependence of v_2 of charged hadrons at different centrality classes for isotropic, jetty and S_T -integrated events in Au+Au collisions at $E_{\text{lab}} = 30A$ GeV.	162
7.13	p_T -dependence of v_3 of charged hadrons at different centrality classes for isotropic, jetty and S_T -integrated events in Au+Au collisions at $E_{\text{lab}} = 30A$ GeV.	162